Influence of magnetic configuration on edge turbulence and transport in the H-1 Heliac

C.A. Michael, F. Zhao, B. Blackwell, M.F.J. Vos[1], J. Brotankova[2], S.R. Haskey[3], B. Seiwald, J. Howard
Australian National University, Canberra, A.C.T. 2601, Australia
[1] *Eindhoven University of Technology, 5600 MB Eindhoven, The Netherlands*
[2] *ARC Centre of Excellence for Coral Reef Studies, James Cook University, Townsville, QLD 4811, Australia and*
[3] *Princeton plasma physics laboratory, Princeton, New Jersey, 08543-0451, USA*
(Dated: 20th February 2017)

The role of the rotational transform (ι) profile on fluctuations and transport is investigated in the H-1 Heliac by means of dynamic (i.e. changing during a shot) and static (fixed during a shot) scans of rotational transform through a range of values where the electron density drops markedly and which correspond to having the point of $\iota_{\min}$ located near $r/a = 0.75$ in a region of magnetic well (such that the surface averaged magnetic field strength increases with radius). The gap is near the $\iota = 4/3$ resonance, but as the resonance is not in the plasma for more than half the gap it is not clear that this is relevant. Although this drop is clearly driven by the variation of helical current, under particular circumstances, similar density changes occur spontaneously. Plasma currents are measured throughout the scan and are found to slightly affect the rotational transform profile, and reverse about the configuration of minimum confinement, whilst induced currents through a toroidal loop voltage in the dynamical scans are not found to be significant. The confinement and fluctuation properties are studied by means of 2D movable Langmuir probes. Large near edge-localised dithering quasi-coherent fluctuations at $\sim 6\,\mathrm{kHz}$ develop in a strong density gradient region with low magnetic shear as ι is scanned up to a point where the density collapses in the outer region. This dithering corresponds to an m=3 mode comprising of standing and propagating components. The net and fluctuation-induced transport components are measured near the plasma edge in a similar discharge, and it is found that fluctuation-induced transport driven by these low frequency coherent modes dominates the particle balance during the low density phase but is only a small component of the net flux when the density is higher.

I. INTRODUCTION

Understanding of the influence of magnetic geometry/topology on confinement and stability is important for next-step and present fusion devices. For example, the suppression/modification of edge localised modes (ELMs) via enlargement/overlap of magnetic islands has been observed in Tokamaks [1], and Stellarators/Heliotrons [2] alike. Furthermore, many examples have been found where the presence of rational surfaces in the plasma has been associated with internal transport barriers [3, 4]. Critical to this understanding is the ability to predict the fundamental dynamics of magnetic island growth/healing [5, 6], and their effect on confinement. Further experimental investigation of the configuration dependence of confinement may help to clarify the important mechanisms. In the LHD Heliotron, ELM events have been linked to resistive interchange modes resonant on a $\iota = 1/1$ magnetic surface, driven by unfavourable magnetic curvature near the edge of the plasma [2]. Strong edge pressure gradients are also essential ingredients for ELMs in both Stellarators and Tokamaks. Studies in low magnetic shear, variable ι devices such as W7-AS [7, 8] and TJ-II [9–12] have thus been invaluable in informing the importance that low order rationals have on confinement (for example, H-mode formation in windows in between low order rationals), and have shown there to be strong instabilities at various windows of ι, exhibiting ELM-like or sawtooth-like dithering events. Whilst events have often been found at rational surfaces, ideal infernal modes, a type of kink-ballooning MHD instability, have been measured in the core of Tokamaks such as MAST, with the mode number of 1/1 mismatching the q profile, with $q_{\min} \sim 1.3$ upon onset [13]. These non-resonant modes are particularly destabilised when the width of the region of low magnetic shear is broad, which is also a feature of a Heliac magnetic configuration. However, the β value required is much higher than that in H-1.

H/He mixture plasma in the H-1 Heliac [14] has also been found to exhibit a similar type of strong variation of plasma density on ι [15]. This plasma is heated by $\sim 40\,\mathrm{kW}$ of (minority) ion cyclotron resonance heating, resulting in plasma parameters of $n_e \sim 3 \times 10^{18}\,\mathrm{m}^{-3}$, $T_i \sim T_e \sim 10\,\mathrm{eV}$. One clear difference of these observations from those mentioned above, is that the plasma density almost completely collapses in certain ι windows showing a very marked effect. Given that, as will be shown in this paper, these losses of confinement are associated with strong instabilities, this prompts the question that, although ELMs themselves have not been shown to have a serious impact on plasma confinement in other Stellarator/Heliotron devices, how can edge-localised plasma instabilities cause such dramatic collapses in density? An obvious question is the role of magnetic hill, as was demonstrated recently in TJ-II [12]. Another puzzling feature from H-1 observations is that the plasma density seems to collapse in a window of ι which is just outside a low-order rational surface, and as such there should be no resonance for an MHD mode or even the formation of any magnetic island. In [15], explana-

tions were given for the various drops in terms of changing amplitude and frequency of magnetic fluctuations, which appeared to show Alfvénic-type frequency scaling with $\omega \sim k_{||}/\sqrt{n_e} \sim \left(\iota - \frac{n}{m}\right)/\sqrt{n_e}$. However, only slight variations in density could be explained, not dramatic drops. These fluctuations have been investigated extensively using data mining techniques [16, 17], and through CAS3D simulations [18, 19], combined with tomography of internal mode structure [20–22], have been identified as β-induced Alfvén eigenmodes (BAEs). Often, there can exist several coherent modes at different frequencies, as well as broadband fluctuations which can be detected much more clearly on Langmuir probes than on the magnetic probe arrays external to the plasma.

Whilst comparison of the mode characteristics with theory is important for validation, an important obvious question remains: what are the impacts of these fluctuations on confinement and how are these related to the anomalous gaps in confinement at certain ι windows? A strong change in the fluctuation-induced flux was shown in the L-H transition observed in low field Helicon wave Ar plasma in H-1 [23]. Langmuir probes have been used in H-1 to measure the electron temperature and density around static island structures under those conditions [24]. Until now, probes have not been used extensively for diagnosing H/He plasma because of the resultant stronger perturbation to the plasma (compared to Ar plasma).

This paper is organised as follows. A new ball-pen probe was developed to measure profiles of ion saturation current (I_{sat}), floating potential, and plasma potential directly and thus the electron temperature, and is discussed in Sec. II. The direct measurement of plasma potential is used to obtain the fluctuation-induced flux in Sec. IV. The role of the helical current (which controls ι) on the electron density is investigated in standard well configurations in Sec. III, by introducing a dynamic scan, i.e. changing the transform during a discharge. This separates the role of plasma formation (the plasma being formed correctly before the helical current is changed), from that of confinement. Such dynamic scan experiments were also conducted on the TJ-II Heliac [25]. The density does drop in a certain ι window and detailed profile variation is analysed, focusing on a dithering behaviour that occurs as the density drops, which has many characteristics of ELMs [2, 8, 11]. The 2D spatial structure of this mode is investigated and it is found to consist of largely counter-propagating m=3 modes, locked to the magnetic configuration. Particle balance analysis is presented in Sec. IV, where the fluctuation-induced flux is compared with the net flux, in a similar discharge to that presented in Sec. III. Finally, discussion and conclusions are presented in Sec. V.

II. BALL-PEN AND CONVENTIONAL PROBE SYSTEMS ON H-1

The main diagnostic for the detailed characterisation of plasma in this paper is a pair of probes. The first, a ball-pen probe [26], is mounted on a 1D movable probe shaft at toroidal angle $\phi = 0°$. Here, the magnetic axis position is at $R = 125$cm and the last closed flux surfaces is around $R = 135$ cm. The minor radial position is denoted by r and a is the minor radius along the same line from the axis. The probe consists of a ceramic shaft of 8mm in diameter with 3 holes of 2mm in diameter each. Molybdenum wire of ∅1.5mm is used as electrodes, protruding 1.5mm for two of the pins measuring V_{fl}, the floating potential, and either I_{sat}, the saturation current or the complete I-V characteristic. The third pin is unique to the ball-pen probe, and is recessed by 4mm (chosen empirically to balance ion and electron currents), to measure V_{pl}, the plasma potential. The electron temperature can be determined from $T_e = (V_{fl} - V_{pl})/3.76$, the coefficient having been determined by comparing with the swept probe (as the theoretical value depends on the effective mass). The probe tends to perturb the plasma when it is inserted more than halfway to the core ($R < 130$ cm). For this reason, this paper focuses on the edge. Whilst I_{sat} is related to electron density and the temperature of both species, no further interpretation is carried out here. Typical profiles of T_e are shown in Fig. (7c). The electron temperature becomes negative, apparently invalid, near the edge where the density drops by an order of magnitude. RF pickup was considered a candidate for this, however, this should have the effect of increasing V_{fl} and thus the temperature (in fact, RF chokes were installed to check this effect). This flat/peaked temperature profile is generally inconsistent with He line ratio measurements [27], which show strongly elevated temperatures in the edge, but is generally consistent in magnitude with probe measurements at mid-radius.

To check the reliability of these ball-pen probe T_e values, measurements were also carried out with a swept single probe, as well as with a triple-probe configuration [28]. These measurements were not available for the shots described in Fig. (7). However, a separate set of experiments was carried out at lower power and in a configuration away from the drop in density ($P_{rf} = 32kW$ and $\kappa_h = 0.83$), with probe measurements carried out in the centre, mid-radius and at the plasma edge. The results are shown in Table (I). For these shots, the same probe tip was configured in different ways. For the swept single probe measurements, fluctuations in V_{fl} and T_e could contaminate the I-V characteristic. For this reason, the sweep rate was set to be 30kHz, however, even then, fluctuations were often present at this frequency. Triple probe measurements are inherently immune to this effect, however the probe tip only had two protruding pins of matching length. Thus, two repeat discharges were carried out, the first one with the probes configured as a biased-double probe

R (cm)	Swept T_e (eV)	Triple T_e (eV)	Ball-pen T_e (eV)
125	30	38	31
130	11	12	11
135	6.9	7.5	2.5

Table I. Comparison of T_e values obtained in different probe configurations, for P_{rf} = 32kW, F_H = 4μTorr, F_{He} = 5μTorr (averaged over t=35-40ms).

(to measure V_+), the second configured as a single floating probe (measuring V_{fl}), from which T_e was evaluated from $(V_+ - V_{fl})/\log 2$. It is clear that in the core and mid-radius (R=125,130cm), there is excellent agreement amongst the three methods. However, at the edge, where the density decreases significantly, the ball-pen probe tends to underestimate the temperature and can even become negative in some instances, as in Fig. (7c). For this reason the ball-pen probe measurements are not considered reliable to measure the details of the temperature profile in regions where the density drops dramatically.

A second conventional probe is installed at ϕ = 7.2°, and can moved be in 2D, both radially and vertically to access a range of positions above the midplane. 3D plasma equilibria computed using VMEC are used to map the probe position to flux coordinates, and can be used to diagnose the spatial structure of turbulence by comparison with the ball-pen probe. To minimise perturbation to the plasma, it consists of only two electrodes on a single ceramic shaft with ∅2 mm, with tungsten electrodes of 0.25 mm in diameter. One of the pins is biased negatively using a battery array to $\approx -130V$ and I_{sat} is measured, whilst the other pin directly measures V_{fl}. For both probe systems, voltages were measured using a voltage divider, with consideration given to maximising the impedance to avoid incorrect readings, but not too high to avoid attenuating fluctuations in the range 100-200kHz.

III. EFFECT OF ROTATIONAL TRANSFORM ON DENSITY

The H-1 flexible Heliac has a helical coil whose current can be varied with a secondary power supply, in order to adjust the ι profile. The ratio of the secondary to primary current, termed κ_h, is the primary control parameter. This behaviour has been studied and analysed in detail in [15]; as κ_h is increased, ι and its profile changes over the range $1 - 1.5$ (plotted in Fig. (1b)). The location of zero magnetic shear moves from the core at $\kappa_h = 0$, outwards up to $r/a \approx 0.6$ at around $\kappa_h = 0.6$, then remaining near that position for higher κ_h. The positions where the zero shear location intersects a low order rational surface are considered to be most unstable from the point of MHD stability. Thus it is these positions which are likely to correspond with poorer confinement (resulting from large scale instability). On the other hand, for standard vertical field

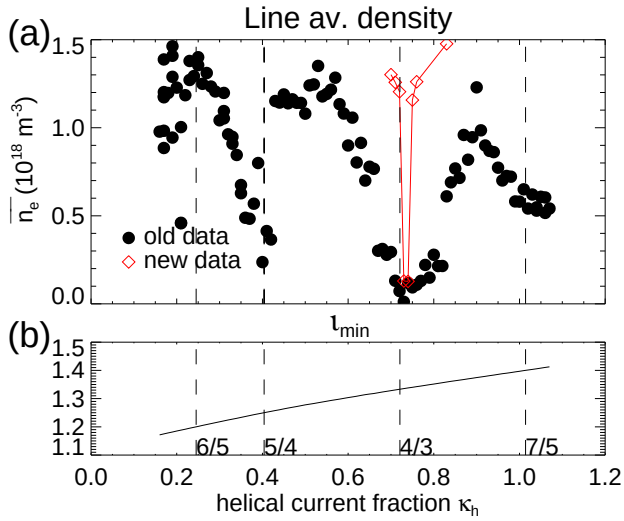

Figure 1. Variation in (a) line-averaged density and (b) minimum rotational transform $\iota_{\min}$ (lower, at zero shear point) as a function of κ_h, for the data-set used to study mode frequency scaling behaviour [16] (P_{rf} = 55kW, F_H = 4μTorr, F_{He} = 5μTorr,) and diamonds for the fixed configurations studied in this paper around the 4/3 resonance (P_{rf} = 53kW, F_H = 10μTorr, F_{He} = 13μTorr).

configurations, the entire radius up to $r/a < 0.8$ is in magnetic well of $\sim 1\%$ while only the very edge is in magnetic hill, thereby producing a stabilising effect for ideal MHD instabilities at the zero shear location.

The line-averaged density, through the plasma centre, from a 140GHz interferometer, is a representative proxy for confinement. A scan of the helical current, with a single shot for each value of κ_h, and the density was taken 50ms into the discharge to be free from transients of plasma formation (the density may peak early in time but fall later in regions of instability) is plotted in Fig. (1), based on the same data-set that was analysed in [16], together with shots taken with the same conditions as dynamical scans studied in Sec. (III A). This information is compared with the minimum ι value for that vacuum configuration in the lower part of the figure. The vacuum ι has been corrected by -0.55% to account for the reduction of ι at high fields (B = 0.5T) as reported in [16]. The vacuum magnetic field model for H-1 has been refined based on extensive electron beam mapping at lower magnetic fields [29].

Figure (1) shows a complex dependence of density on rotational transform. The configurations with low order rational surfaces at the position of $\iota = \iota_{\min}$ (having zero magnetic shear) are indicated with dashed lines. Confinement degradation produced by low order rational surfaces in the plasma should occur on the lower side of these critical values of κ_h, when the rational ι is inside the plasma, and the ι profile crosses a rational surface twice. While this reasoning fits well with the 5/4 resonance, it is difficult to understand the drop in the range $\kappa_h \sim 0.72 - 0.8$ most of which is on the high side

of the resonance. Because this is the largest unexplained feature, this paper analyses new measurements focusing on this region. There have been some upgrades since the original work, notably the RF antenna shape has been modified to better match the plasma, but the behaviour is similar. The gap is in the same place, and at higher filling pressures of Hydrogen and He F_H, F_{He}, or heating powers P_{rf}, it becomes narrower.

A. Helical current scans near the large gap

Motivated by these results in static shots, dynamic scans, where κ_h (and hence ι) is varied during the shot were undertaken initially in order to clarify whether the low density was a result of poor plasma formation, or some intrinsic instability in the discharge. The waveform of κ_h is programmed to be initially 0.72, where, according to the static scan, the plasma density is still high, and κ_h is ramped up to 0.82 over the following 90ms at which point the RF heating pulse is terminated. The time trace of the line-averaged density, helical current fraction and ion saturation current at different radial locations is plotted for the entire discharge, in Fig. (2). After plasma formation, the initial line-averaged density is high, but decreases as κ_h is ramped before recovering again. The κ_h values corresponding to the time window with the drop in density appear to match the same values where the drop occurs in the fixed scan shown by the in red diamonds of Fig. (1). Here, the drop in density is only moderate ($\approx 20-30$) whereas the density drops by an order of magnitude in the static scan. One can thus conclude that the degradation is not caused by lack of plasma formation, rather it is due to an intrinsic effect, for example an instability, that arises at a particular values of κ_h. Examining the $I_{\rm sat}$ traces for the entire discharge in Fig. (2b) and in Fig. (3) for time windows during the density drop (8-28ms) and at the plasma formation stage (2-7ms), it can be seen that the drop appears to be localised here in peripheral regions ($r/a \approx 0.7$). Furthermore, associated with the drop, there appears to be very large dithering type fluctuations in the saturation current, which increase at the drop, particularly in the time range 15-20ms for R=132cm in Fig. (3a). However, they also appear to increase in the recovery phase at $t \sim 50-60$ms in Fig. (2b). These dithering events are characterised in Sec. (IIIC). As these occur simultaneously with the drop in density, they may be either the cause of effect of the density drop. There is also, however, evidence that instabilities arise during plasma formation in Fig. (3b), initially near the edge of the plasma (R=133-134cm) at around 4ms, shortly after which the local values of I_{sat} start to decrease. However the instability does not appear (initially) for lower radii.

Whilst the fluctuation-induced flux could not be accurately calculated for this discharge, an indicator of the relative contribution can be estimated based on $\int i\mathcal{F}(I_{sat}(t))\mathcal{F}^*(V_{fl}(t))\omega d\omega$ (for segmented time windows, similar to Eq. (4)). This value is given in Fig. (4), for R=132cm, compared with I_{sat} at that location. This flux estimate excludes the consideration of the value and direction of k_θ (equivalently the poloidal phase velocity), and does not properly exclude T_e fluctuations (which, according to the results in Sec. (IV), can lead to phase shifts which result in a reversal of the flux direction, thus producing an offset from the true flux). It is clear that the flux estimate increases in magnitude as the drop is occurring, as well as during the recovery phase, though we cannot be certain of the direction. However, a more thorough interpretation would require taking into account complex spatial dependencies and better probe measurements. A more quantitative analysis is carried out for a very similar discharge in Sec (IV), where it is shown that dithering fluctuations of similar frequency can produce a particle flux which is a large fraction of the net flux during a time window in which the line-averaged density is low.

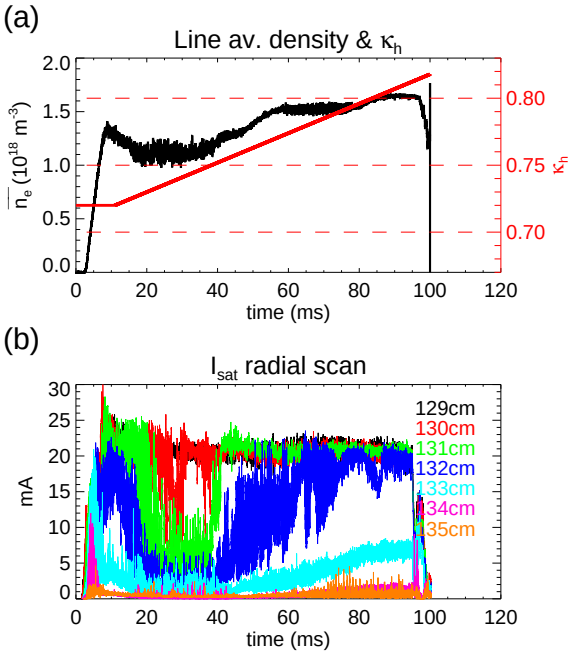

Figure 2. (a) Line-averaged density and helical current fraction wave-forms, and (b,c) I_{sat} for various major radial positions (R_{ax} = 125cm, R_{LCFS} = 135cm) for the helical current scan shot with P_{rf} = 53kW, $F_H = 10\mu$Torr and $F_{He} = 13\mu$Torr.

The key novel feature about these κ_h scan discharges is that the density is forced to drop particularly near the edge and does not collapse everywhere. Wave-forms of line-averaged density and κ_h, for a set of discharges with static κ_h as well as the dynamically scanned discharge are plotted in Fig. (5). It is clear that for $\kappa_h = 0.73$, 0.74 (green and dark blue in Fig. (5a)), the line-averaged density decreases much more strongly than in the scan. On the other hand, for $\kappa_h = 0.75$ (cyan trace), the line-averaged density starts out low, but recovers gradually over time (which cannot be explained by

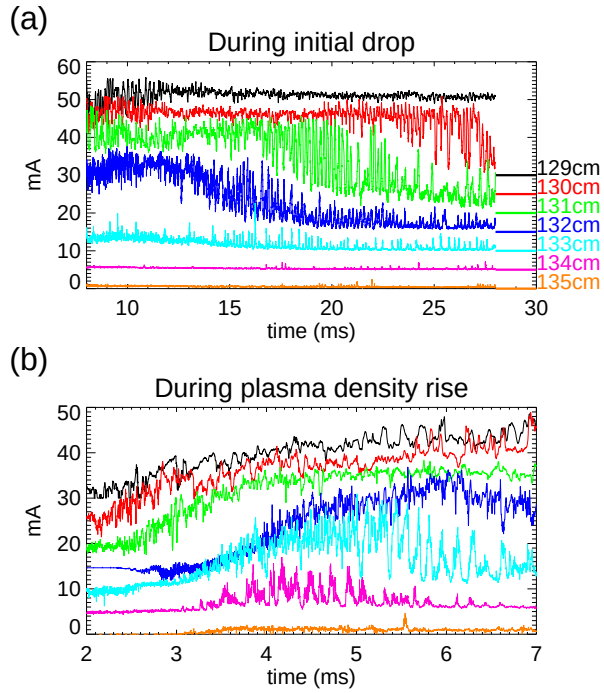

Figure 3. Detailed view of $I_{sat}(t)$ for various radial positions during (a) the initial density drop and (b) during the plasma startup phase. The different radial locations have been offset from each other for clarity, and the offset is indicated at the right side of (a).

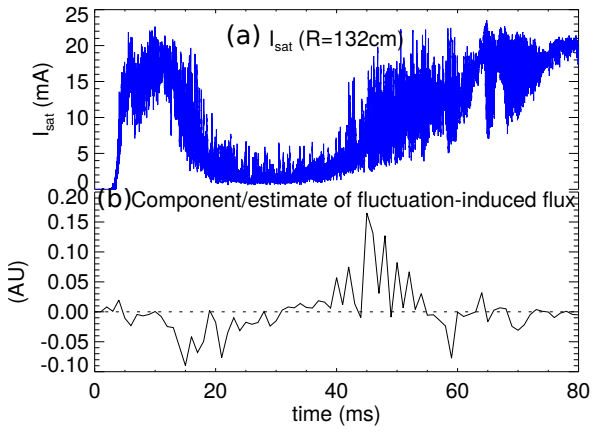

Figure 4. (a) I_{sat}, at R=132cm (blue trace in Fig. (2)), compared with (b) an estimation of a component of the fluctuation-induced flux (as described in text). As V_{fl} is used rather than V_{pl}, and since the turbulence propagation direction is not accounted for, we cannot be certain about the direction of the flux.

changes in plasma current) and importantly demonstrates that near values of κ_h associated with the density drop, the density and fluctuation amplitude can change in time without the direct influence of changing rotational transform. Furthermore, for certain discharge types (such as in Sec. (IV)), this time-evolution can be influenced by the depth to which the probe is inserted into the plasma. Thus it can be concluded that the magnetic configuration has

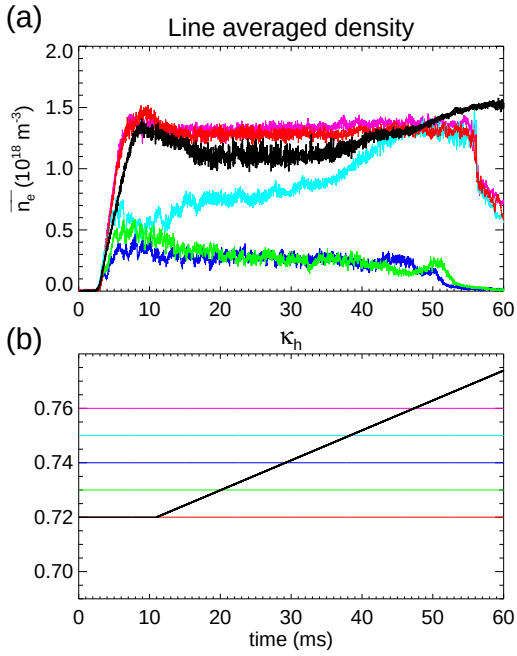

Figure 5. (a) Line-averaged density and (b) helical current fraction κ_h as functions of time for a set of static κ_h discharges (colours), as well as a dynamic scan discharge (black).

an influence on turbulence which in turn affects the plasma density. However, there are also other factors influencing the evolution of the turbulence, particularly near certain values near the edges of the κ_h window for the density drop.

A more detailed comparison of the line-averaged density as a function of $\iota_{\min}$, in both static and dynamic scans, in the vicinity of the targeted density drop is given in Fig. (6a). For the static scan, the shots indicated by red diamonds in Fig. (1) were repeated in order to measure the toroidal plasma current, however the conditions were not completely identical leading to a less severe drop in density, but with the same κ_h dependence. Dynamic scans of the helical current may be subject to extraneous plasma currents driven by the counter-electromotive force generated by increasing the poloidal flux, which may in turn affect the ι profile. This effect is found to be quite significant in dynamic configuration scans in the the TJ-II Heliac, and can generate kA of current [25]. Furthermore, it was also shown on TJ-II that runaway electrons could be generated during the main coils ramp up phase (i.e. before initiation of the plasma), which, if not attenuated properly using a mechanical paddle, could contribute to the plasma current [30]. However, no such system was used in these experiments on H-1.

It is clear that the $\iota_{\min}$ dependence of the density is very similar between the static and dynamic scans, indicating that this inductive current component is insignificant. Rogowski measurements in dynamic scans (carried out over a different range of κ_h where the plasma hardly changes) show that for the same

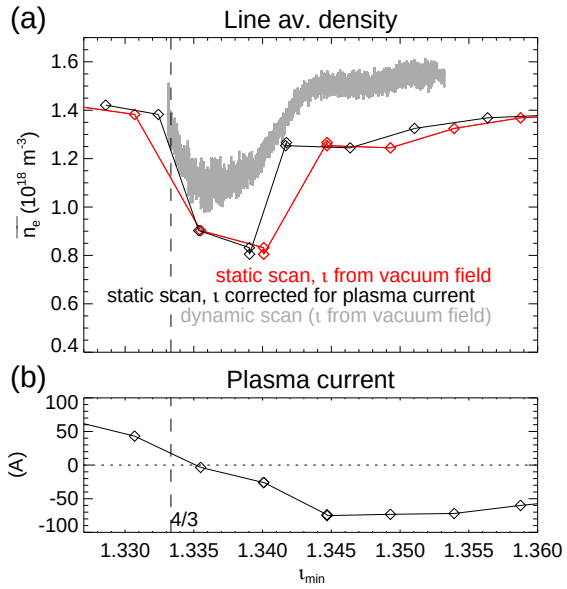

Figure 6. Comparison of static and dynamic configuration scan, and evaluation of role of plasma current on ι. (a) Line-averaged density as a function of $\iota_{\min}$ for (points) averaged over 50-60ms of the a set of discharges with constant κ_h in time ($P_{rf} = 59kW$, $F_H = 10\mu$Torr and $F_{He} = 13\mu$Torr), with the red points taken using the vacuum field configuration and black points using an approximate correction for the plasma current and for (grey line) taken from the dynamic configuration scan with the vacuum field configuration. (b) Plasma current as a function of the (plasma current corrected) $\iota_{\min}$ in the static scan (black points).

swing rate of the helical coil current, a counter current of ~ 10A is generated. It is likely that hysteresis and particle confinement time are more critical for dynamic scans, since for configurations near the density drop, the density can be variable in time.

The measured plasma current for the static scan is observed to change direction from the co to the counter direction as $\iota_{\min}$ is increased through the region of the density drop. The magnitude of this current has a small but significant effect on the ι profile. Using a simple cylindrical approximation, assuming that all of the current is contained within the radius of the 4/3 rational surface, the change in $\iota_{\min}$ is calculated and is indicated by the black line in Fig. (6a). Because of the reversal of the current, the width of the density gap is actually reduced by this plasma current but still remains above the 4/3 resonance, implying that there must be some finite parallel component to the wave-number for the mode to be resonant.

B. Profile changes throughout the helical current scan

In order to better understand the driving mechanisms for the changes in density, radial profiles of density and temperature were obtained with the ball-pen probe. These changes can then be compared with the profiles of ι and magnetic well assess the MHD stability. The time history of the saturation current from the ball-pen probe at a range of different radii is plotted in Fig. (2d). It is clear that there is a strong abrupt change in the density at $R = 132$ cm whilst there is a much smaller change at $R = 130$ cm, and virtually no change at $R = 129$ cm, indicating that there is a strong gradient at this position. It is also clear that the plasma undergoes very dramatic dithering cycles at $R = 132$ cm on the way down in the drop, at $t = 15$ms and as the density is rising, at $t \sim 40$ ms. There is also a dithering at $R = 130$ cm at $t \sim 25 - 30$ ms.

Radial profiles of I_{sat}, T_e and ι and well are plotted on the same abscissa in Fig. (7). Different time intervals are used: $27.5 - 32.5$ ms, indicative of the density during the drop, $7.5 - 12.5$ ms, prior to the drop, and the limits of the I_{sat} dithering over a time interval just as the drop occurs. It is clear that prior to the crash, the I_{sat} profile is broader, with the position of maximum gradient around R=132cm, whilst during the crash, the position of maximum gradient is around 130.5cm. The relative change in density is largest at R=132cm, and small both in the core and near the edge . The values of T_e are only plotted where the local I_{sat} value is $> 50\%$ of the maximum value, as it was found in Sec (II) that near the edge, where the density is low, the ball-pen probe delivers erroneous values of T_e. These profiles can be compared with ι and well profiles. The position of zero magnetic shear is at R=131.5cm, which is exactly in the middle between the positions of maximum gradient of the I_{sat} profiles prior and during the density crash, i.e. where the dithering behaviour is strongest, and its onset coincides with the presence of the 4/3 rational surface at the zero shear position as in Fig. (6a). The magnetic well profile shows that a magnetic hill only exists in the region $R > 134.5$ cm, and so, this may not be playing a significant role here, particularly as the relative change in density near the periphery is close to zero.

C. Characterisation of dithering behaviour associated with the density drop

As the dithering behaviour in the saturation current seems to occur at the same time as the density is dropping, characterisation of this phenomenon may help to understand the reasons for the gap in confinement in the region $\kappa_h = 0.72 - 0.8$. It has already been established in Fig. (7a) that the dithering is strongest radially over the position of zero magnetic shear. Here, through the use of two probe signals, one of which can move poloidally, the 2D structure is investigated. Also, a 1D photo-multiplier tube (PMT) array was configured to measure line-integrated spectral line emission across the plasma. This was initially set-up to measure H_α, as this is often used as a measure of edge phenomena, particularly, ELMS, in high temperature plasma, and was used as an effective diagnostic of edge transport

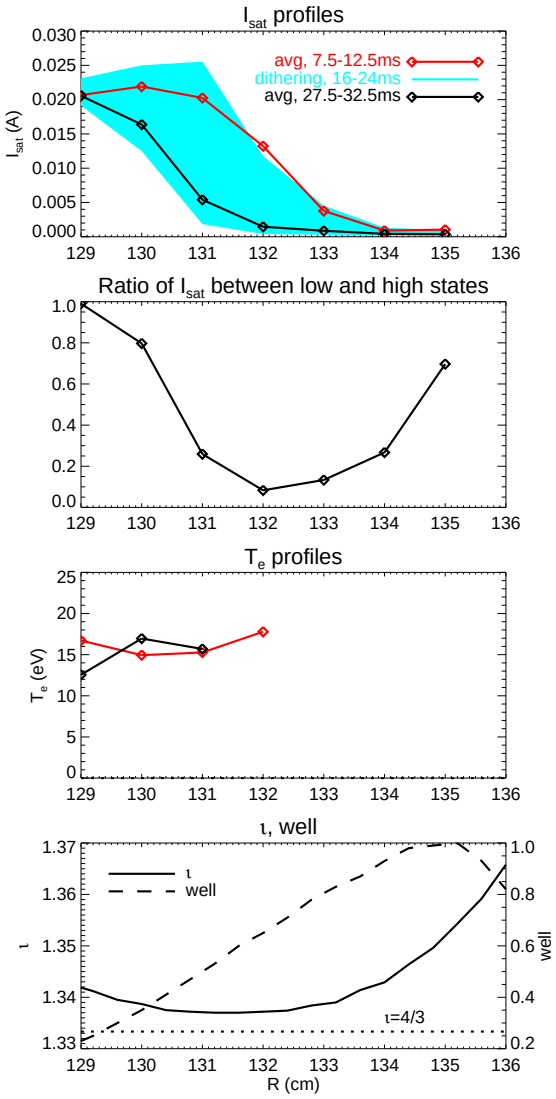

Figure 7. (a) saturation current, profiles during different time intervals prior, after and during the dithering density drop (the limit cycles indicated by the envelope of the filled blue region), (b) ratio of I_{sat} during the density drop to that before the drop, (c) Electron temperature (measured using ball-pen probe) and (d) ι and well profiles at $\kappa_h = 0.72$. The magnetic axis is at $R = 125\,\mathrm{cm}$ and the last closed surface is at $R = 135\,\mathrm{cm}$.

events in TJ-II [11]. However, in H-1, because of the relatively low temperatures, neutral hydrogen penetrates to the core of the plasma and the signals are less intrinsically edge localised. It was found that C II emission at 514nm, which has been shown to be more strongly related to the electron density than temperature in these regimes [20], was brighter and so was used here.

Figure (8) shows time histories of the probe signals (the two placed on the same flux surface, at the same field line), as well as a contour plot of the C II emission from the PMT array. The quasi-coherent oscillation at $\approx 6\,\mathrm{kHz}$ is apparent here from the time history. Particle flux produced by this strong instability may contribute to keeping the density lower in

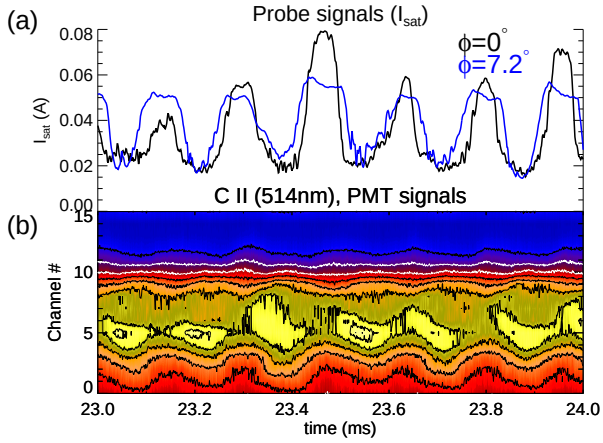

Figure 8. Zoomed-in view of dithering behaviour at density crash in κ_h scan. (a) Probe signals at R=132cm, $\phi = 0°$(r/a=0.7), and on the same flux surface and same field line, but on the other probe at $\phi = 7.2°$. (b) Contour plot of the C II light emission, line integrated from a photo-multiplier tube array, looking across the short direction of the plasma at $\phi = 155°$.

this phase. Because of its edge localisation, it has many similarities with ELMs/edge harmonic oscillations observed on TJ-II [11] and W7-AS [8]. The time traces are not completely identical on either probe which may be due slight alignment issues with the probes, however, it may relate to some more intrinsic properties about variation of the oscillation along the field line. The light emission from the PMT array clearly shows the same bursting like behaviour, albeit with phase lag, which may be accounted for by the difference of toroidal angle, and, the position of the peak shifts throughout the oscillation cycle, apparently moving downwards in the figure. However, rather than moving upwards, the peaks tend to flatten out and on most cycles the upward movement is not well pronounced. This type of behaviour is different from that of a rotating instability, which would have equally strong propagation in either direction and tend to look like a zig-zag pattern. Additionally, magnetic probe arrays on H-1 do not show any 6kHz component (though it does modulate higher frequency fluctuations).

The PMT array is informative because it can take continuous high speed projections of the plasma emission, however line-integration effects make the interpretation difficult, particularly for such temporally oscillating structures which may have finite m and n numbers. A Langmuir probe on the other hand, is very localised but does not provide an overall picture of the turbulence structure, unless the probe is moved shot-by-shot. Using the two probes described in Sec. II, the ball-pen probe (with signal I_1) is fixed (at $z = 0, \phi = 0$) and the second conventional probe is moved ($I_2(R, Z)$) within a poloidal plane ($\phi = 7.2°$), in order to map out the correlation function of I_{sat} for this 6kHz quasi-coherent mode. For each shot with a different position of the 2D movable probe, the time window was adjusted slightly around $t = 20$ms to account for variability

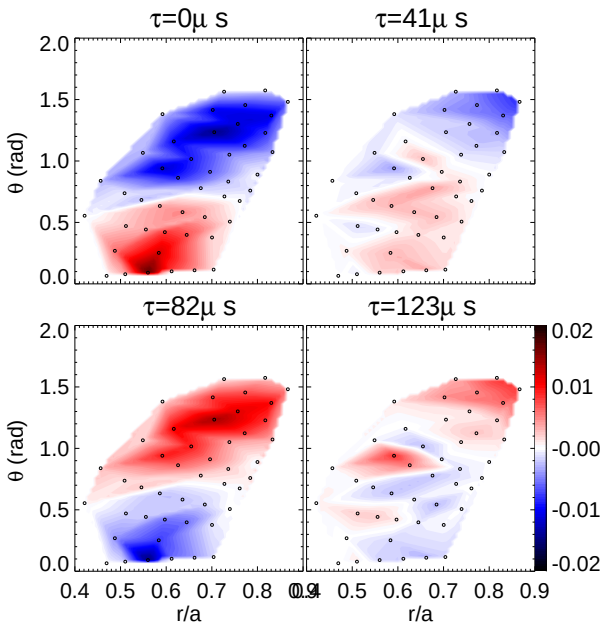

Figure 9. Cross-correlation of I_{sat} between fixed probe pairs at $r/a = 0.55$, (normalized to show AC part of oscillation of movable probe), in flux coordinates at time intervals of 41μs, corresponding to 1/4 period of the 6kHz oscillation. Flux surfaces are vertical lines in this coordinate system, and dots represent the points where measurements were made (each one a separate discharge).

in the starting time of the dithering.

The results of this calculation are presented in Fig. (9). Four temporal frames are presented corresponding to an entire period of the oscillation. It is clear that at $\tau = 0$, the density is highly peaked on the flux surface towards θ=0 and inverts for $\theta \geq 0.8$. At a quarter period later ($\tau = 41\,\mu$s), the amplitude of the oscillation is much weaker, whilst at $\tau = 82\,\mu$s, the oscillation has reversed with respect to $\tau = 0$. Finally, at at $\tau = 123\,\mu$s, the oscillation is weaker again. In addition to these trends, the amplitude of the fluctuation does not appear to align perfectly with the flux surfaces, which may be an artefact of the probe perturbation. In this manner, it becomes clear that the density peak does not propagate, and the pattern has clear features of a standing wave.

To indicate more clearly the standing wave nature of this oscillation, a slice is taken at $r/a = 0.55$, and a contour plot of I as a function of θ and τ is plotted in Fig. (10). Whilst there may be multiple Fourier components, the most striking feature is a pattern with m=3. As a standing wave would have zero response in the middle (i.e near $\theta = 0.6$),the finite response tends to indicate the presence of a propagating component, in other words, that wave components in opposite directions are not completely balanced. This complicates the evaluation of the fluctuation-induced particle flux as a standing wave should produce no net radial flux. To avoid this difficulty, in Sec. (IV), a clearly propagating mode was

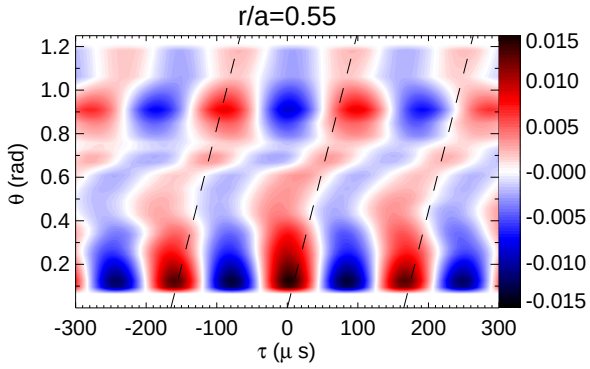

Figure 10. Temporal and poloidal angle dependence of the normalised I_{sat} cross-correlation function, at $r/a = 0.55$. Dashed lines indicate the expected propagation phase front for a pure m=3 mode.

analysed. In fact,preliminary indications of other discharges with slightly different RF antenna conditions (position and relative phase of the two antenna elements) show a completely propagating wave. This different behaviour may indicate that the plasma is near a threshold for mode locking to the vacuum fields. The m=3 propagating component has a phase velocity of 1.4 km/s which is typically of the order of the ExB velocity obtained from ball-pen probe measurements of V_{pl}.

IV. PARTICLE BALANCE ANALYSIS

To understand the role of fluctuations in producing the density drop as shown in Sec. (III), particle balance analysis is carried out by computing the total flux as well as the fluctuation induced flux to clarify its relative contribution. The net flux Γ_{net} is computed by solving the particle balance equation:

$$\frac{dn(r)}{dt} + \nabla \cdot \Gamma_{net}(r) = S(r), \qquad (1)$$

where S is the ionisation rate. Whilst the ionization rate could be computed from knowledge of the filling neutral pressure and the plasma profiles, it is easier to measure the absolute irradiance of H/He neutral spectral lines, and infer the ionization based on a tabulated S/XB number [31], where the density and temperature ranges are obtained from the ball-pen (and swept) probe. (Using this technique, the results are not as strongly sensitive to errors of temperature or density as complete modelling would be.) The ionization rate is related to the optical emissivity $\epsilon(r)$, via $S(r) = \frac{S}{XB}(r).\epsilon(r)$. Time dependent line-integrated projections of the emissivity for H_α(656nm) and He I emission line at 667nm were obtained using an imaging spectrometer and CCD array. These were then fitted to a model for $\epsilon(r) = \text{const}$ (for $r < a$), to take account of the line-integration effect. (Whilst this may not be strictly true, the fit to the data is reasonable). Eq. (1) is then inverted to determine the flux at the edge of the plasma:

$$\Gamma_{net}(a) = \frac{1}{2}\frac{S}{XB}\epsilon a \qquad (2)$$

For the results presented here, the $\mathrm{d}n/\mathrm{d}t$ term has been neglected, which is justified during the flat-top periods. The contributions for H and He are added (It is assumed that He only exists in its first ionization stage, because there is no measurable He II light which would tend to also indicate further ionization). It was found that He contributes $\sim 2\times$ that of H in this mixed plasma. Furthermore, in results below, this ratio was assumed to be constant, as the He light was not measured in the dithering discharge.

The fluctuation-induced flux is computed using the formula $\Gamma_{fl} = \langle \tilde{n}\tilde{v}_r \rangle$, where $\tilde{v}_r$ is the radial velocity associated with the fluctuation $\tilde{E}_\theta \times B$ velocity. Expressing $\tilde{n}$ and $\tilde{v}_r$ as a inverse Fourier transforms (operator $\mathcal{F}^{-1}$) over k_θ, the poloidal wavenumber, and writing $\tilde{E}_\theta = ik_\theta \tilde{V}_{pl}$, one obtains

$$\Gamma_{fl} = \langle \mathcal{F}^{-1}(\tilde{n}(k_\theta))\mathcal{F}^{-1}(\tilde{V}_{pl}(k_\theta).ik_\theta/B)\rangle \qquad (3)$$

Using the assumption $k_\theta = \omega/v_{ph}$, where v_{ph} is the poloidal phase velocity and ω the angular temporal frequency, and invoking Parseval's theorem, the flux can be expressed as

$$\Gamma_{fl} = \int_{-\infty}^{\infty} iP_{nV}(\omega).\frac{1}{B}\frac{\omega}{v_{ph}}d\omega \qquad (4)$$

where $P_{nV}(\omega) = \mathcal{F}(n(t))\mathcal{F}^*(V(t))$ is the cross-power spectrum between density and plasma potential. For computing the above equation, v_{ph}, was determined using the time delay cross-correlation technique applied to the I_{sat} signals of two (toroidally and poloidally) separated pairs of probes as described in Sec. (IIIC), on field lines that were separated by 100mm poloidally. For these measurements, the ball-pen probe was located in the high gradient zone near the edge, at $R = 132\,\mathrm{cm}$. For the time window 30-40ms in results below, the phase velocity was 7km/s in the ion diamagnetic direction, the correlation coefficient obtained was 0.75. The ball-pen probe signal (the recessed pin) was used for $\tilde{V}_{pl}$ and the density fluctuation was obtained from $\tilde{I}_{sat}$ (using the interferometer and probe scan data to obtain the effective area, and assuming constant temperature).

Whilst it would be desirable to use the discharge analysed in Sec. (III), V_{pl} data was subject phase-shifts in the electronics for that discharge. These effects were mitigated in later discharges making the analysis possible. The most interesting result of this analysis was obtained for a discharge with very similar fluctuation behaviour, with a magnetic well over the entire plasma, obtained using 25% less vertical field. The time history of the line-averaged density, κ_h, the I_{sat} signal, and the flux analysis (Γ_{net} and Γ_{fl}) is plotted in Fig. (11).

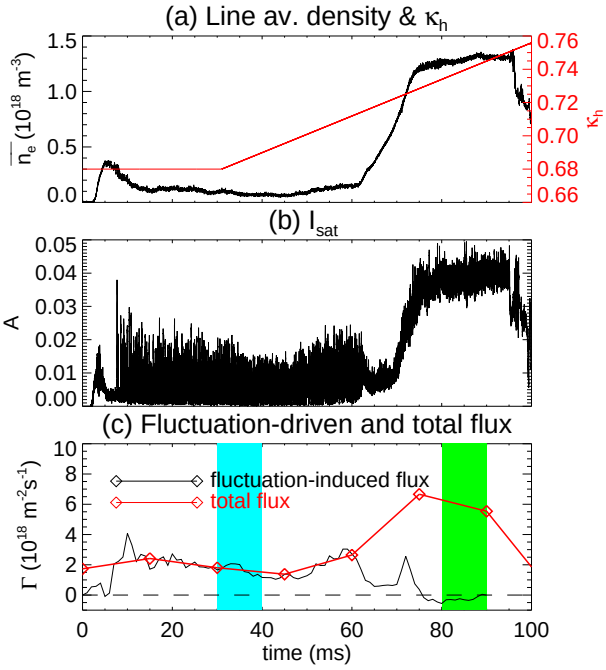

Figure 11. Time history for κ_h scan shot with decreased vertical field (larger well, more stable) with $P_{rf} = 53$kW, $F_H = 10\mu$Torr, $F_{He} = 13\mu$Torr. (a) Line-averaged density and κ_h evolution. (b) I_{sat} at R=132cm. (c) Net flux at the edge of the plasma (uncertainty 30%), and fluctuation-induced flux at R=132cm (positive is outwards, uncertainty 20%). The two time-windows designate steady periods of low and high confinement (30-40 and 80-90ms)

Just after start-up, large fluctuations appear slightly after the local density has dropped and the line-averaged density is coming down, however, data from other radii show quite different temporal behaviour on account of probe perturbation. Consequently, no conclusion about the the causality of the drop can be obtained, however, a local steepening of the pressure profile as the line averaged density is going down could give rise to this type of behaviour.

The reduced vertical field has the effect of slightly shifting the ι profile for fixed κ_h, thus the "gap", or region of low density, has shifted from $\kappa_h = 0.72$ to 0.68. During the first part of the discharge ($t < 60$ms), the fluctuation-induced flux of $2\times10^{18}\mathrm{m}^{-2}\mathrm{s}^{-1}$ almost exactly matches the net flux. Note the accuracy in the net fluctuation flux estimates is only about $\sim 30\%$, on the basis of the assumptions used in the analysis as described above (for example, the simplified Abel inversion method) and is inaccurate during the density rise/fall phase because the dn/dt term is neglected. Furthermore, the fluctuation-induced flux may in fact be variable along the flux surface which could also contribute some further uncertainty to the fluctuation-induced flux, and this uncertainty is likely to be of the order of 20%.

At $t = 60\,\mathrm{ms}$, the fluctuation amplitude and fluctuation-induced flux starts to decrease at the

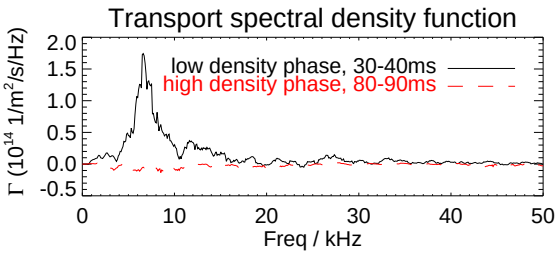

Figure 12. Comparison of frequency spectra of the transport spectral density function (integrand on RHS of Eq. (4)) for intervals during the low density phase and high density phase of the discharge in Fig. (11), showing that a coherent mode at $\sim$ 7kHz is responsible for the flux.

same time that the line averaged density, and net flux increases. By $t = 90$ms, the fluctuation-induced flux has reduced to $-0.5 \times 10^{18}\mathrm{m}^{-2}\mathrm{s}^{-1}$(inwards) compared with the net flux of $6 \times 10^{18}\mathrm{m}^{-2}\mathrm{s}^{-1}$ (outwards). This change in fluctuation-induced flux (of -125%) and the net flux (of 200%) is larger than the 20% and 30% uncertainty in the flux estimates in the early phase of the discharge.

The two facts: (a) the contribution of at least 50% the total flux by fluctuation-induced flux (considering the 30+20% uncertainty), and (b) the reduction in fluctuation-induced flux when the line-averaged density increases demonstrate that fluctuation-induced transport contributes greatly to limiting the density in the first phase of the discharge (8-60ms), though the trigger for such fluctuations excitation and suppression is not clear.

Note that the fluctuation induced flux direction reverses and its magnitude increases by an order of magnitude if V_{fl} is used, i.e. if the temperature fluctuations are not accounted for (which the ball-pen probe does by balancing ion and electron currents by having the pin recessed in the ceramic). Recently, a comparative study was carried out of the fluctuation properties and flux from ball-pen and conventional Langmuir probes [32] in the ISTTOK boundary plasma. It was shown that, whilst the plasma potential from ball-pen probes is free from the effects of electron temperature fluctuations, the amplitude may be smaller and thus underestimate the magnitude of plasma potential fluctuations. In that study it was shown that the direction of the flux was the same whether the floating or plasma potential was used, in contrast to the result here.

The transport spectral density (frequency dependence of the flux) as in Eq. (2) is compared for time intervals in the low and high density phase for this shot in Fig. (12). Here it is clear that in the low density phase, a large flux is driven by a mode at 7kHz, providing further corroboration that the dithering mode is in fact responsible for the degradation in confinement. Whilst the vertical field in this shot is different, it shows that the same type of mechanism may be responsible. Furthermore, since this configuration has *increased* well, it further shows that this mechanism is unlikely to be related to magnetic hill.

V. DISCUSSION AND CONCLUSION

An investigation was carried out as to the reasons for the unexpected large "gap" in confinement in the range $\kappa_h = 0.72 - 0.8$ at standard vertical field. It was found that at higher neutral gas filling pressure, that gap could be condensed into a much narrower region in the range 0.72-0.74, and that the plasma current reverses from lower to higher κ_h, about a point very close to which $\iota_{\min} = 4/3$ (within reasonable experimental uncertainty). Dynamic scans in κ_h were carried out, over the range 0.72-0.82 within a single shot, and it was found that the drop in confinement occurred over the same range in κ_h (0.72-0.74), and was not strongly affected by currents induced by the changing magnetic field. Similar large changes in density may appear spontaneously (without changes in ι) when the configuration is close to that at which the transition between low and high density states occurs (e.g. κ_h= 0.75 in Fig. (5)). The scan revealed that this density crash occurred when the position of strongest pressure gradient was very close to the position of zero magnetic shear and was associated with a strong quasi-coherent mode localised within a normalised width $\Delta\rho = 0.2$ of this position. This quasi-coherent mode was shown to comprise standing and propagating components, the results shown in Fig. (9) show a dominance of a standing wave, however other discharges show propagating modes, possibly indicating proximity to a mode locking threshold. Because of their edge localisation and proximity to magnetic hill regions, as well as their temporal character, they are similar to ELMs observed in other Stellarator devices. However, the regions where the mode and density drop are localised are not far out enough to be explained by magnetic hill as in LHD [2]. It was significant to identify a regime where only partial collapse of the line-averaged density occurred for certain κ_h values, revealing changes near the edge of the plasma and the zero-shear position.

In the standard vertical field, the fluctuation-driven flux analysis was not accurate enough to determine whether it was responsible for the drop in density. However, pronounced changes occurred to the magnitude of the flux at the time of the drop. Furthermore, fluctuations excited near the periphery of the plasma resulted in an immediate decrease in the local density (Fig (3b)). More quantitative particle balance analysis was possible on a mode in a very similar configuration, with larger magnetic well. In this discharge, at the same radius, the density was low initially but recovered later as κ_h was increased. Fluctuation-induced flux accounts for a large part of the flux, despite uncertainty and assumptions in the analysis. Thus one hypothesis for the collapse in density is that fluctuation-induced flux produced by quasi-coherent modes at a few kHz is sufficient to overcome ionization, however more detailed analysis and a reduction of the uncertainties would be necessary to prove this. As the plasma density is a balance of ionization and particle losses (includ-

ing due to fluctuations), it may be that at lower gas fill or lower power, the ionization rate would be lower and thus any fluctuation driven at the start of the discharge could prevent the density from rising significantly. This may explain why the original observations at lower neutral density showed a drop in density over a broad range of κ_h compared with discharges carried out here.

Because analysis is only carried out at certain radial locations (on account of plasma perturbation as the probe is moved), there are more details about the density profile evolution which have not been revealed here. In particular, it is noteworthy to question the causality of the fluctuations, whether they are a result of the changing profiles due to density drop itself, or whether they are a result directly of the changing κ_h values and proximity to the 4/3 resonance in the ι profile. Either way, the experimental fact is that these type of fluctuations only appear in discharges with $\iota_{\min}$ close to the 4/3 rational surface.

It is significant that that the large crash in confinement should only occur with the ι profile just above the 4/3 rational surface (within half a percent, as shown in Fig. (6)). As this is associated m=3 wave modes, they must have a finite value of $k_{||}$. The infernal kink mode [13] is one such example of a non-resonant mode, however the plasma β in H-1 is quite low. Also the mode is driven unstable in a region of magnetic well, indicating that a it is stable to ideal MHD modes. It is also surprising that the flux should be produced by a large scale mode (m=3): normally, it is only considered possible for there to be an appreciable phase lag between density and potential for scales approaching the ion gyro-radius ($\sim 5\,$mm in these discharges). However, resistive drift waves, which can be be included in an MHD description may also allow such a phase lag, and may also produce instability in a region of magnetic well.

One particular feature about ι in this configuration is that this is the only really low order rational to have a zero shear point located close to the gradient zone near the edge. Lower values of κ_h have ι profiles which are more monotonically increasing from the core, and will be the subject of future work. Identification of the propagation direction of turbulence in the plasma frame from precise measurements of the fluctuation velocity, as well as $v_{E\times B}$ will be the focus of future investigations. In addition to studying different ι windows, further investigations of configurations with increased and decreased well will be carried out to understand the link to, and role of, resistive interchange modes.

VI. ACKNOWLEDGEMENTS

This work was supported in part by the Education Investment Fund under the Super Science Initiative of the Australian Government, the National Collaborative Research Infrastructure Strategy (NCRIS) and by the Australian Research Council Discovery grant number DP120103153. The authors also gratefully acknowledge technical support provided by Mark Gwenyth and Michael Blacksell.

[1] T. E. Evans, R. A. Moyer, P. R. Thomas, J. G. Watkins, T. H. Osborne, J. A. Boedo, E. J. Doyle, M. E. Fenstermacher, K. H. Finken, R. J. Groebner, M. Groth, J. H. Harris, R. J. La Haye, C. J. Lasnier, S. Masuzaki, N. Ohyabu, D. G. Pretty, T. L. Rhodes, H. Reimerdes, D. L. Rudakov, M. J. Schaffer, G. Wang and L. Zeng, Physical Review Letters **92** (2004) (23), p. 235003

[2] K. Toi, S. Ohdachi, Y. Suzuki, F. Watanabe, K. Tanaka, S. Sakakibara, K. Ogawa, M. Isobe, X. D. Du, T. Akiyama, M. Goto, K. Ida, S. Masuzaki, T. Morisaki, S. Morita, K. Narihara, Y. Narushima, T. Tokuzawa, I. Yamada, R. Yasuhara, M. Yoshinuma, K. Kawahata, H. Yamada and L. H. D. E. G. the, Nuclear Fusion **54** (2014) (3), p. 033001

[3] M. E. Austin, K. H. Burrell, R. E. Waltz, K. W. Gentle, P. Gohil, C. M. Greenfield, R. J. Groebner, W. W. Heidbrink, Y. Luo, J. E. Kinsey, M. A. Makowski, G. R. McKee, R. Nazikian, C. C. Petty, R. Prater, T. L. Rhodes, M. W. Shafer and M. A. Van Zeeland, Physics of Plasmas **13** (2006) (8), p. 082502

[4] K. Ida, Y. Sakamoto, M. Yoshinuma, H. Takenaga, K. Nagaoka, N. Hayashi, N. Oyama, M. Osakabe, M. Yokoyama, H. Funaba, N. Tamura, K. Tanaka, Y. Takeiri, K. Ikeda, K. Tsumori, O. Kaneko, K. Itoh, S. Inagaki, T. Kobuchi, A. Isayama, T. Suzuki, T. Fujita, G. Matsunaga, K. Shinohara, Y. Koide, M. Yoshida, S. Ide, Y. Kamada, L. H. D. E. G. the and J. T. T. the, Nuclear Fusion **49** (2009) (9), p. 095024

[5] R. Fitzpatrick and F. L. Waelbroeck, Physics of Plasmas **19** (2012) (11), p. 112501

[6] S. Nishimura, Physics of Plasmas **21** (2014) (12), p. 122502

[7] R. Brakel, M. Anton, J. Baldzuhn, R. Burhenn, V. Erckmann, S. Fiedler, J. Geiger, H. J. Hartfuß, O. Heinrich, M. Hirsch, R. Jaenicke, M. Kick, G. Kühner, H. Maaßberg, U. Stroth, F. Wagner, A. Weller, W. A. Team, E. Group and N. B. I. Group, Plasma Physics and Controlled Fusion **39** (1997) (12B), p. B273

[8] M. Hirsch, P. Grigull, H. Wobig, J. Kisslinger, K. McCormick, M. Anton, J. Baldzuhn, S. Fiedler, F. Ch, J. Geiger, L. Giannone, H. J. Hartfuss, E. Holzhauer, M. Hirsch, P. Grigull, H. Wobig, J. Kisslinger, K. McCormick, M. Anton, J. Baldzuhn, S. Fiedler, F. Ch, J. Geiger, L. Giannone, H. J. Hartfuss, R. Jaenicke, M. Kick, H. Maassberg, F. Wagner, A. Weller and W. A. S. T. the, Plasma Physics and Controlled Fusion **42** (2000) (5A), p. A231

[9] T. Estrada, L. Krupnik, N. Dreval, A. Melnikov, S. M. Khrebtov, C. Hidalgo, B. v. Milligen, F. Castejón, E. Ascasíbar, L. Eliseev, A. A.

Chmyga, A. D. Komarov, A. S. Kozachok and V. Tereshin, Plasma Physics and Controlled Fusion **46** (2004) (1), p. 277

[10] T. Estrada, F. Medina, D. López-Bruna, E. Ascasíbar, R. Balbín, A. Cappa, F. Castejón, S. Eguilior, A. Fernández, J. Guasp, C. Hidalgo and S. Petrov, Nuclear Fusion **47** (2007) (4), p. 305

[11] D. López-Bruna, M. A. Ochando, A. López-Fraguas, F. Medina and E. Ascasíbar, Nuclear Fusion **53** (2013) (7), p. 073051

[12] A. M. d. Aguilera, F. Castejón, E. Ascasíbar, E. Blanco, E. D. l. Cal, C. Hidalgo, L. Bin, A. López-Fraguas, F. Medina, M. A. Ochando, I. Pastor, M. A. Pedrosa, B. V. Milligen and J. L. Velasco, Nuclear Fusion **55** (2015) (11), p. 113014

[13] I. Chapman, M.-D. Hua, S. Pinches, R. Akers, A. Field, J. Graves, R. Hastie and C. Michael, Nuclear Fusion **50** (2010) (4), p. 045007

[14] S. M. Hamberger, B. D. Blackwell, L. E. Sharp and D. Shenton, Fusion Science and Technology **17** (1990) (1), pp. 123–130

[15] J. H. Harris, M. G. Shats, B. D. Blackwell, W. M. Solomon, D. G. Pretty, S. M. Collis, J. Howard, H. Xia, C. A. Michael and H. Punzmann, Nuclear Fusion **44** (2004) (2), p. 279

[16] B. D. Blackwell, D. G. Pretty, J. Howard, R. Nazikian, S. T. A. Kumar, D. Oliver, D. Byrne, J. H. Harris, C. A. Nuhrenberg, M. McGann, R. L. Dewar, F. Detering, M. Hegland, G. I. Potter and J. W. Read, *Configurational Effects on Alfvenic modes and Confinement in the H-1NF Heliac*, in *IAEA FEC*, pp. EX/P9–11, also in arXiv:0902.4728

[17] S. R. Haskey, B. D. Blackwell and D. G. Pretty, Computer Physics Communications **185** (2014) (6), pp. 1669–1680

[18] J. Bertram, M. J. Hole, D. G. Pretty, B. D. Blackwell and R. L. Dewar, Plasma Physics and Controlled Fusion **53** (2011) (8), p. 085023

[19] J. Bertram, B. D. Blackwell and M. J. Hole, Plasma Physics and Controlled Fusion **54** (2012) (5), p. 055009

[20] S. R. Haskey, B. D. Blackwell, C. Nührenberg, A. Könies, J. Bertram, C. Michael, M. J. Hole and J. Howard, Plasma Physics and Controlled Fusion **57** (2015) (9), p. 095011

[21] S. R. Haskey, B. D. Blackwell, B. Seiwald and J. Howard, Nuclear Fusion **54** (2014) (8), p. 083031

[22] S. R. Haskey, N. Thapar, B. D. Blackwell and J. Howard, Review of Scientific Instruments **85** (2014) (3), p. 033505

[23] M. G. Shats and D. L. Rudakov, Physical Review Letters **79** (1997) (14), pp. 2690–2693

[24] S. T. A. Kumar, B. D. Blackwell, J. Howard and J. H. Harris, Physics of Plasmas **17** (2010) (8), p. 082503

[25] D. López-Bruna, J. A. Romero, R. Jiménez-Gómez, M. A. Pedrosa, M. Ochando, T. Estrada, A. López-Fraguas, F. Medina, J. Herranz, T. Kalhoff, E. Ascasíbar, A. d. l. Peña, F. Lapayese and J. Alonso, Nuclear Fusion **49** (2009) (8), p. 085016

[26] J. Adámek, J. Stöckel, M. Hron, J. Ryszawy, M. Tichý, R. Schrittwieser, C. Ionită, P. Balan, E. Martines and G. V. Oost, Czechoslovak Journal of Physics **54** (2004) (3), pp. C95–C99

[27] S. L. Ma, J. Howard, B. D. Blackwell and N. Thapar, Review of Scientific Instruments **83** (2012) (3), p. 033102

[28] S. Chen and T. Sekiguchi, Journal of Applied Physics **36** (1965) (8), pp. 2363–2375

[29] S. T. A. Kumar, B. D. Blackwell and J. H. Harris, Nuclear Fusion **49** (2009) (3), p. 035001

[30] L. Rodríguez-Rodrigo, F. Medina, M. A. Ochando and A. López-Fraguas, *Generation of fast electrons in TJ-II*, in *26th EPS Conf. on Contr. Fusion and Plasma Physics*, pp. 353 – 356

[31] D. Nishijima, R. P. Doerner, M. J. Baldwin, E. M. Hollmann, R. P. Seraydarian and Y. Ueda, Physics of Plasmas **14** (2007) (10), p. 103509

[32] C. Silva, J. Adamek, H. Fernandes and H. Figueiredo, Plasma Physics and Controlled Fusion **57** (2015) (2), p. 025003